Original Research Paper

Evaluation of mechanical properties of nanoparticles using a constant-volume shear tester

Yasuhiro Shimada, Kai Yamamura, Shuji Matsusaka *

Department of Chemical Engineering, Kyoto University, Kyoto 615-8510, Japan

ABSTRACT

Nanoparticles have advantageous small-size and surface effects that impart them with unique mechanical properties. To evaluate these properties, a constant-volume shear tester that can precisely measure stresses on the shear plane was used. Six samples, namely, hydrophilic and hydrophobic silica, alumina, and titania nanoparticles, were prepared for the shear tests. For each sample, a single shear test provided the void fraction, stress relaxation ratio, stress transmission ratio, powder yield locus, consolidation yield locus, critical state line, shear cohesion, and flow function. All the tests were conducted under ambient conditions using powder beds, in which the void fractions were in the range of 0.89–0.96. A series of analyses demonstrated that the hydrophilic nanoparticles have lower flowability than the hydrophobic nanoparticles, indicating that moisture on the surface increases the cohesion and inhibits the flow.
© 2019 The Society of Powder Technology Japan. Published by Elsevier B.V. and The Society of Powder Technology Japan. This is an open access article under the CC BY-NC-ND license (http://creativecommons.org/licenses/by-nc-nd/4.0/).

1. Introduction

Nanoparticles have attracted attention as functional materials in various industries, including the chemical, pharmaceutical, and food industries. Owing to small-size and surface effects, nanoparticles exhibit unique mechanical properties. Commonly, nanoparticles are applied to impart fluidity to powders [1–4] and to increase material strength by kneading them into soft materials such as plastics and rubbers. However, to utilize nanoparticles effectively, a deeper understanding of their mechanical properties is necessary.

Powder manufacturing processes require several unit operations, e.g., storage, supply, and transportation of the powders. These operations change the void fractions and stresses in powders. High stresses lead to the failure of powder beds, thus initiating particle motion. This behavior depends on external factors such as vibration [5–8], electric field [9], temperature [10,11], humidity [12], moisture [13–15], and particle morphology [16–18]. Therefore, knowledge about the mechanical properties is extremely useful for achieving smooth performance of these operations.

Test methods for evaluating the mechanical properties of powders differ between low- and high-stress conditions. Under low-stress conditions, methods relying on measurements of the angle of repose, compressibility, angle of spatula, cohesion (or uniformity) [19], and flow behavior [6–8,20] are used. However, owing to external mechanical forces on powders under high stresses, methods that evaluate the relationship between the stresses and the flow behavior are more desirable. In particular, the shear test is suitable because it allows evaluation of the phenomena associated with the failure of powder beds under compression. Two test types, i.e., the constant-load shear test and the constant-volume shear test, are available. The Jenike shear tester [21,22], which is a representative tester for the former, uses weights to apply a normal stress to the powder bed for compression. However, as this test must be performed several times under various weights to obtain the powder yield locus (PYL), the procedure is complex. In addition to the Jenike shear tester, other shear testers that use parallel plates, rotational cells, etc. are available [23–28]. As an alternative to the constant-load shear test, the constant-volume shear test was proposed as a simple and easy-to-operate method [29–33]. This method is characterized by a constant volume throughout the shear operation. Therefore, the void fraction of the powder bed remains constant during shearing and the continuous changes in the normal and shear stresses can be simultaneously measured. As a result, the PYL can be acquired using a single shear test.

Specifications for shear tests have been stipulated in American Society for Testing and Materials Standards [34,35] and Japanese Industrial Standards [36]. The measurement methods have been compared [37–39], and the difference in the preconsolidation stresses has been examined [40]. These methods have also been applied to pharmaceutical prescriptions [41–43].

* Corresponding author.
E-mail address: matsu@cheme.kyoto-u.ac.jp (S. Matsusaka).

Nomenclature

C	shear cohesion (Pa)
F	force (N)
f_c	unconfined yield strength (Pa)
ff_c	$= \sigma_1/f_c$ (–)
t	time (s)
D_p	nominal particle diameter (m)
γ_{RS}	stress relaxation ratio (–)
γ_{T1}	stress transmission ratio between the top and shear planes at steady-state shear (–)
ε	void fraction (–)
ρ_p	particle density (kg/m³)
σ	normal stress (Pa)

σ_1	major consolidation stress, i.e., major principal stress given by the Mohr stress circle of steady state flow (Pa)
τ	shear stress (Pa)
φ_{CSL}	angle of critical state line (°)

Subscripts

H	horizontal
L	lower
P	powder
S	shear plane
U	upper
V	vertical

Recently, the measurement accuracy of shear tests has been remarkably improved. An apparatus based on the constant-volume shear test was developed to include both a load cell that measures the normal stress for powder compression and a load cell that measures the normal stress working on the shear plane [32,33]. Using this apparatus, the effects of stress relaxation and transmission were examined and a method was proposed to obtain both the PYL related to expansion failure and the consolidation yield locus (CYL) related to consolidation failure [32]. Based on the stress balance, a method was reported for measuring the normal stress on the shear plane and the effect of the structural properties of the apparatus, including the powder bed height and cell diameter [33].

Although shear tests have been used to measure the mechanical properties of nanoparticles, a limited number of reports are available [44]. In the present work, we quantitatively analyzed the mechanical properties of nanoparticles using the constant-volume shear tester with a focus on the differences in the surface characteristics, i.e., hydrophilicity and hydrophobicity, of silica, alumina, and titania nanoparticles.

2. Materials and methods

2.1. Shear tester

Fig. 1 shows the structure of the constant-volume shear tester. The shear cell consists of an upper stainless-steel cylinder of 40 mm in height with an inner diameter of 30 mm and a lower base with a recessed section of 5 mm in depth and the same diameter. A vertical servo motor compresses the powder bed by vertically moving a piston (0.2 mm/s), and the load cell on the piston measures the upper vertical force (F_{VU}). The lower section of the shear cell and the sides contain two load cells that measure the lower vertical force (F_{VL}) and the horizontal shear force (F_H). These three forces are converted into the upper normal stress on the powder bed (σ_U), the normal stress on the shear plane (σ_S), and the shear stress (τ). Although the upper section of the shear cell is fixed to the body of the apparatus, the lower section is installed on a two-axis stage. The powder bed is sheared by moving this stage using a horizontal servo motor at a constant speed (10 μm/s). The height of the powder bed and the horizontal shear displacement are measured using two non-contact laser displacement sensors. Owing to the presence of a 0.05 mm gap, the upper and lower sections of the shear cell are independent of each other. When the shear cell is not filled with powder, the mechanical friction in the lower section during horizontal movement is <0.3 kPa, which is negligible compared with the shear stress. During experiments, we adjusted the initial vertical force conditions so that σ_S = 20, 30, and 40 kPa. The height of the powder bed was 20 ± 1 mm.

Fig. 1. Structure of the constant-volume shear tester.

2.2. Samples

Table 1 summarizes the properties of the samples, namely, hydrophilic and hydrophobic silica, alumina, and titania nanoparticles (Evonik Japan). As the nanoparticles, which were manufactured via gas-phase reactions, were in an agglomerated state, the nominal particle diameters provided by the manufacturer are given. The samples were kept at a temperature of 18 ± 4 °C and a relative humidity of 40% ± 10%. All the experiments were conducted under the same ambient conditions.

2.3. Experimental procedure

Fig. 2 shows the time sequence of the shear test for a representative sample. As the details are described in a previous report [33], we only provide a summary here. From top to bottom, Fig. 2 shows the temporal changes in the upper vertical force (F_{VU}), the lower vertical force (F_{VL}), and the horizontal shear force (F_H). The values of F_{VU} and F_{VL} increase during the compression process (i). The friction between the powder and the upper side wall of the shear cell results in different values for F_{VU} and F_{VL}. After compression, the sample is left for a period of 150 s, and F_{VU} and F_{VL} decrease during

Table 1
Powder properties.

Surface modification	Material	D_p (nm)[*]	ρ_p (kg/m³)	Moisture (mass%)[**]
Hydrophilic	SiO₂	16	2200	≤1.5
	Al₂O₃	13	3900	≤5.0
	TiO₂	21	4200	≤1.5
Hydrophobic	SiO₂	16	2200	≤0.5
	Al₂O₃	13	3900	≤2.0
	TiO₂	21	4200	≤1.0

[*] Nominal particle diameter.
[**] Loss on drying after 2 h at 105 °C.
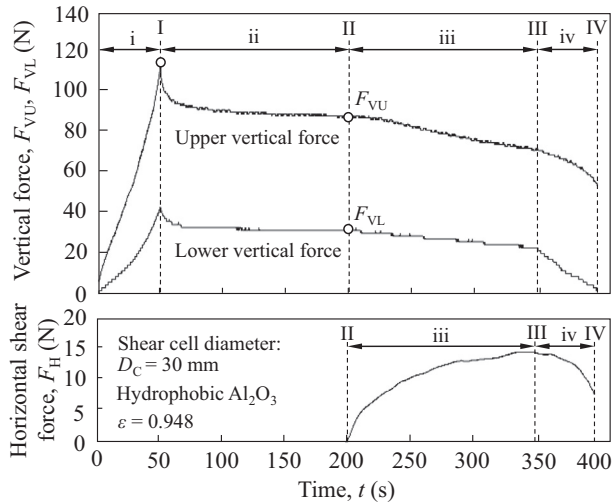
Fig. 2. Time sequence of the shear test.

the stress-relieving process (ii). After the shearing process begins, F_H increases and then approaches a constant value, whereas the normal stress further decreases, as indicated by the consolidation failure process (iii). The two-axis stage is slowly lowered during the shearing process; consequently, F_{VL} decreases to zero and F_H decreases to a certain value, as indicated by the expansion failure process (iv). The values of σ_S and τ are obtained from the values of F_{VL} and F_H. Subsequently, CYL and PYL are obtained from σ_S and τ in processes (iii) and (iv) of the single shear test.

2.4. Parameters for evaluating powder flowability

When the powder bed is compressed in the vertical direction, an internal stress gradient is formed. The particles change their position and orientation to reduce the stress gradient, thus relieving the stress [32,33]. To evaluate the mechanical properties associated with the stress relaxation, we defined a stress-relaxation ratio (γ_{RS}) using the maximum normal stress on the shear plane (σ_{S0}) and the normal stress after stress relaxation (σ_{S1}), as follows:

$$\gamma_{RS} = 1 - \frac{\sigma_{S1}}{\sigma_{S0}} \tag{1}$$

Another mechanical property is the stress transmission in the powder bed. The stress transmission ratio γ_{T1} after stress relaxation was defined based on the normal stress on the shear plane (σ_{S1}) and the upper normal stress (σ_{U1}), as follows:

$$\gamma_{T1} = \frac{\sigma_{S1}}{\sigma_{U1}} \tag{2}$$

The constant-volume shear tester allows the PYL to be easily obtained and is thus suitable for evaluating the shear cohesion (C) and the flow function (FF). C, which corresponds to the

y-intercept of the PYL, depends on the void fraction of the powder bed and is correlated to the unconfined yield strength (f_c).

The FF obtained from the PYL is also widely used to evaluate powder flowability. The FF describes the relationship between f_c and the major consolidation stress (σ_1) and can be evaluated using ff_c, as defined by the following equation:

$$ff_c = \frac{\sigma_1}{f_c} \tag{3}$$

The guidelines for flowability can be summarized as follows: $1 < ff_c < 2$: very cohesive; $2 < ff_c < 4$: cohesive; $4 < ff_c < 10$: easy flowing; and $ff_c > 10$: free flowing [26].

3. Results and discussion

3.1. Stress relaxation ratio

Fig. 3 shows the relationship between the stress relaxation ratio (γ_{RS}) and the normal stress (σ_{S1}). The stress relaxation ratios are in the range of 0.1–0.4. When σ_{S1} increases, γ_{RS} decreases because the stress gradient in the powder bed increases with the increase in σ_{S1}, resulting in rapid rearrangement of the particles. Thus, stress relaxation begins during compression of the powder bed, causing a relative decrease in the stress relaxation ratio with over time. The decrease in γ_{RS} associated with the increase in σ_{S1} is more notable at high γ_{RS} values. In other words, the σ_{S1} dependence tends to decrease with a decrease in γ_{RS}. This behavior occurs because the degree of freedom associated with particle rearrangement is small in powders with low γ_{RS} values.

The hydrophilic nanoparticles (open symbols, Fig. 3) clearly have lower γ_{RS} values than the hydrophobic nanoparticles (closed symbols, Fig. 3). Water molecules adsorbed on the surfaces of hydrophilic nanoparticles strengthen the interactions among particles, increasing the cohesion and inhibiting particle rearrangement.
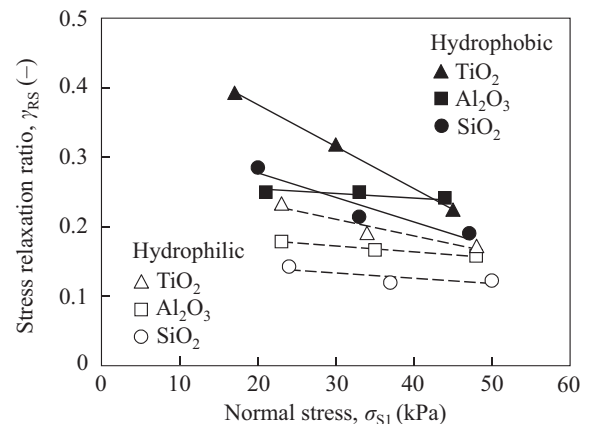
Fig. 3. Stress relaxation ratio of powder beds.

3.2. Stress transmission ratio

Fig. 4 shows the relationship between the stress transmission ratio (γ_{T1}) and the normal stress (σ_{S1}). The normal stresses on the shear plane are 40–70% of the upper normal stress. Some of the vertical stress is converted into horizontal stress; subsequently, friction between the particles and the upper side wall of the shear cell decreases the stress transmission ratio. For all the samples, γ_{T1} increases with an increase in σ_{S1}. This behavior occurs because an increase of the normal stress causes the void fraction of the powder bed to decrease; consequently, the rigidity of the powder bed increases. Although there was a clear difference in γ_{RS} between the hydrophilic and hydrophobic particles (Fig. 3), no significant difference in γ_{T1} was observed between the hydrophilic (open symbols, Fig. 4) and hydrophobic (closed symbols, Fig. 4) nanoparticles. The result indicates that the effect of the nanoparticle diameter was notable and that the ratio of the effect on the sidewall of water molecules adsorbed on the nanoparticle surface was small. Thus, the hydrophobic and hydrophilic effects were not clearly observed.

3.3. PYL, CYL, CSL, and shear cohesion

Shear tests were conducted for the hydrophilic and hydrophobic silica, alumina, and titania nanoparticles (Figs. 5–7), and the major results determined for all the samples, i.e., normal stress σ_{S1}, void fraction ε, shear cohesion C, critical state line (CSL) angle φ_{CSL}, unconfined yield strength f_c, major consolidation stress σ_1, and ff_c (ratio between f_c and σ_1), are summarized in Table 2.

Fig. 5 shows the shear test results for the silica nanoparticles. Although the void fraction (ε) is larger than 0.92, strong friction exists between the particles. In addition, it is worth noting that the shear stress increases significantly with a slight decrease in ε because of the strong cohesive properties of the nanoparticles. The ε values of the hydrophilic particles are larger than those of the hydrophobic particles. In addition, the CSL angles (φ_{CSL}) of the hydrophilic and hydrophobic particles are 44° and 38°, respectively, indicating that the hydrophilic particles have lower flowability. Furthermore, for the hydrophilic particles, the shear cohesion (C) values are approximately twice as high as those of the hydrophobic particles, i.e., $C = 18$–20 for hydrophilic particles and $C = 7$–10 for hydrophobic particles. This result clearly demonstrates the difference in interparticle cohesion caused by moisture.

Fig. 6 shows the shear test results for the alumina nanoparticles. Similar to the silica nanoparticles, the hydrophilic particles exhibit lower flowability than the hydrophobic particles, and the two φ_{CSL} values are different, i.e., 48° and 31° for hydrophilic and hydropho-
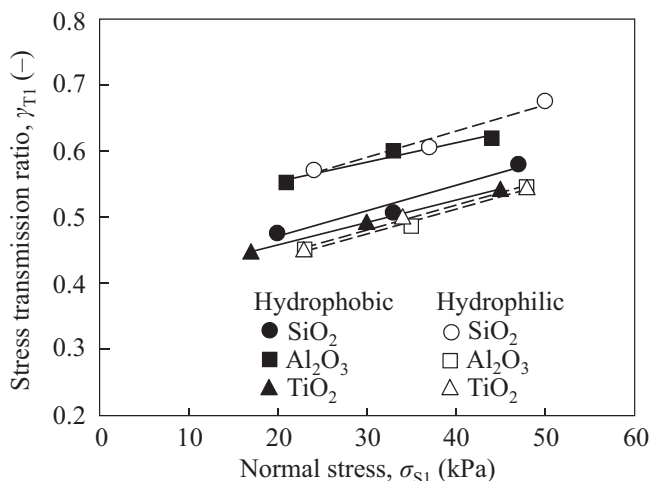
Fig. 4. Stress transmission ratio of powder beds.
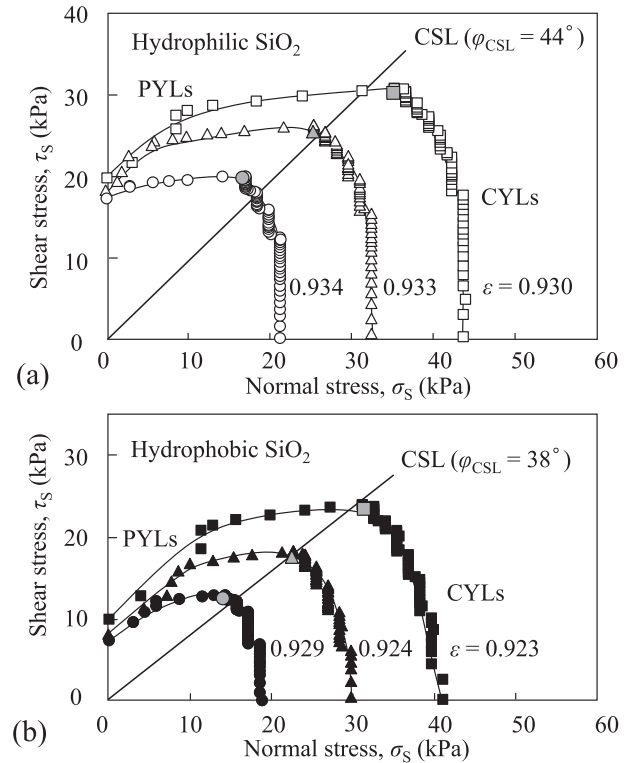
Fig. 5. Shear test results (τ_S–σ_S plots) at various void fractions (ε): (a) hydrophilic SiO$_2$ and (b) hydrophobic SiO$_2$.
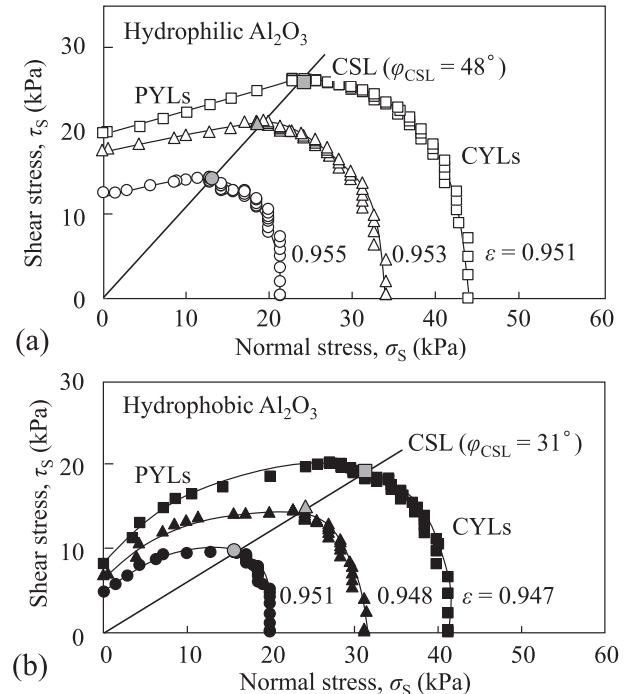
Fig. 6. Shear test results (τ_S–σ_S plots) at various void fractions (ε): (a) hydrophilic Al$_2$O$_3$ and (b) hydrophobic Al$_2$O$_3$.

bic particles, respectively. In addition, the C values of the hydrophilic particles are approximately twice as high as those of the hydrophobic particles.

Fig. 7 shows the shear test results for the titania nanoparticles. Similar to the other nanoparticles, the hydrophilic particles have higher C values than the hydrophobic particles. However, the φ_{CSL}
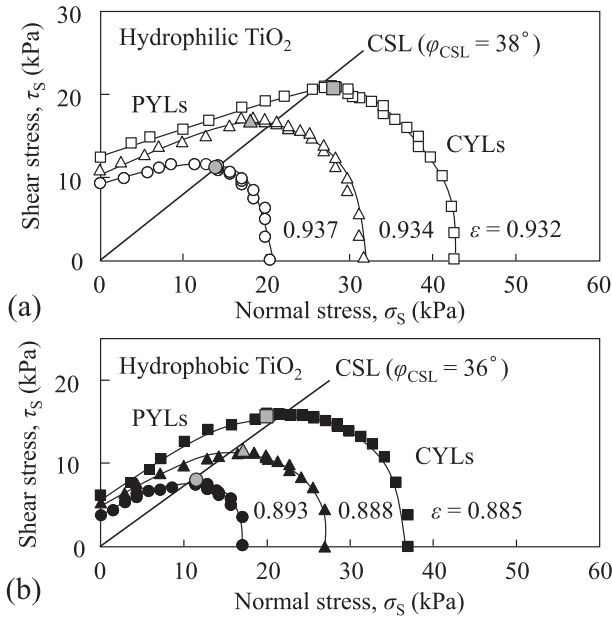
Fig. 7. Shear test results (τ_S–σ_S plots) at various void fractions (ε): (a) hydrophilic TiO$_2$ and (b) hydrophobic TiO$_2$.

Fig. 8. Shear cohesion of hydrophilic and hydrophobic nanoparticles.
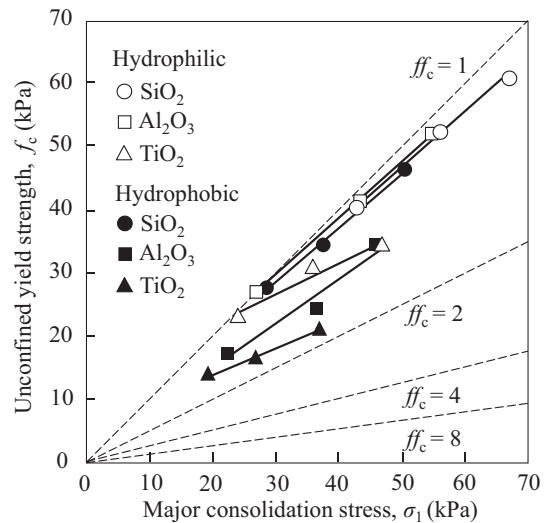
Fig. 9. Flow functions (f_c–σ_1 plots) of hydrophilic and hydrophobic nanoparticles and lines of constant flowability ff_c. The broken lines represent ff_c = 1, 2, 4, and 8.

values of the hydrophilic and hydrophobic titania nanoparticles are similar (38° and 36°). As no clear difference was observed, the effect of hydrophilicity and hydrophobicity on φ_{CSL} is minor. As the void fraction of the hydrophobic titania nanoparticles was rather small ($\varepsilon \approx 0.89$), the agglomeration structure might be different from that of the other nanoparticles.

Fig. 8 shows a comparison of all the samples in terms of the shear cohesion. The C values increase with an increase in the normal stress. Notably, the C values of the hydrophilic nanoparticles are higher than those of the hydrophobic nanoparticles, decreasing in the order of silica, alumina, and titania. As discussed earlier, moisture can increase particle cohesion, and this effect is reflected in the C values.

3.4. Flow function

From the results shown in Figs. 5–7, we obtained the unconfined yield strength (f_c) and the major consolidation stress (σ_1), the value of which were used to determine the FFs, as presented in Fig. 9. As all the values fall between ff_c = 1 and 2, all the nanoparticle samples can be considered "very cohesive". However,

FF results also indicate that the flowability of the hydrophilic nanoparticles tends to be lower than that of the hydrophobic nanoparticles. Powder flowability is often evaluated by the FF obtained from the PYL. Using the present apparatus, the PYL and FF can be easily obtained in a single shear test.

Table 2
Summary of experimental results.

Surface modification	Material	σ_{S1} (kPa)	ε (–)	C (kPa)	φ_{CSL} (°)	f_c (kPa)	σ_1 (kPa)	ff_c (–)
Hydrophilic	SiO$_2$	21.2	0.934	17.5	44	40.2	42.9	1.0
		32.5	0.933	18.2		52.0	56.0	1.0
		43.9	0.930	20.0		60.8	66.4	1.1
	Al$_2$O$_3$	21.2	0.955	12.1	48	26.9	27.2	1.0
		34.0	0.953	17.4		41.1	43.3	1.0
		43.9	0.951	19.9		51.8	54.7	1.0
	TiO$_2$	19.8	0.937	8.9	38	22.7	23.8	1.1
		32.5	0.934	10.2		30.5	35.9	1.3
		42.4	0.932	12.6		33.9	46.9	1.5
Hydrophobic	SiO$_2$	18.4	0.929	7.4	38	27.3	28.4	1.0
		29.7	0.924	8.3		34.3	37.5	1.2
		41.0	0.923	10.4		46.1	50.4	1.2
	Al$_2$O$_3$	19.8	0.951	5.1	31	17.4	22.6	1.1
		31.1	0.948	6.6		23.9	36.8	1.3
		41.0	0.947	8.5		34.2	45.8	1.4
	TiO$_2$	17.0	0.893	3.7	36	13.4	19.1	1.7
		26.9	0.888	4.7		16.1	26.8	1.5
		36.8	0.885	5.8		20.7	36.7	1.6

4. Conclusions

We used a constant-volume shear tester that can precisely measure the normal stress on the shear plane to examine the effect of surface characteristics on the mechanical properties of silica, alumina, and titania nanoparticles. The results obtained can be summarized as follows:

(1) The void fractions of the powders after compression were in the range of 0.89–0.96, with the hydrophilic nanoparticles exhibiting larger void fractions than the hydrophobic nanoparticles.

(2) The stress relaxation ratios (γ_{RS}) were in the range of 0.1–0.4 and decreased with an increase in normal stress. Moreover, the hydrophilic nanoparticles demonstrated lower γ_{RS} values than the hydrophobic nanoparticles because water molecules adsorbed on the surface strengthened the interactions among particles, thus increasing cohesion and inhibiting particle rearrangement.

(3) The stress transmission ratios (γ_{T1}) were in the range of 0.4–0.7 and increased with an increase in the normal stress. However, no significant difference in γ_{T1} was observed between the hydrophilic and hydrophobic nanoparticles.

(4) The PYL, CYL, and CSL results indicated that the hydrophilic nanoparticles have lower flowability than the hydrophobic nanoparticles.

(5) The shear cohesion (C) of the hydrophilic nanoparticles was approximately twice as high as that of the hydrophobic nanoparticles.

(6) The ratios of the major consolidation stress to the unconfined yield strength (ff_c) were between 1 and 2, indicating that the examined nanoparticle samples were "very cohesive". However, the FFs indicated that the flowability of the hydrophilic nanoparticles tends to be lower than that of the hydrophobic nanoparticles.

(7) This series of experiments verified the effectiveness of the constant-volume shear tester for evaluating the flowability of nanoparticles.

References

[1] F. Fulchini, U. Zafar, C. Hare, M. Ghadiri, H. Tantawy, H. Ahmadian, M. Poletto, Relationship between surface area coverage of flow-aids and flowability of cohesive particles, Powder Technol. 322 (2017) 417–427.

[2] J.-J. Park, E.-K. Park, G.-J. Lee, C.-K. Rhee, M.-K. Lee, Effect of a nano-sized TiC particle addition on the flow-assisted corrosion resistance of SA 106B carbon steel, Appl. Surf. Sci. 415 (2017) 143–148.

[3] Y.-N. Zheng, H.-F. Lu, X.-L. Guo, X. Gong, Study on the effect of nanoparticles on the bulk and flow properties of granular systems, Fuel Process. Technol. 177 (2018) 30–38.

[4] J. Rudén, G. Frenning, T. Bramer, K. Thalberg, G. Alderborn, Relationships between surface coverage ratio and powder mechanics of binary adhesive mixtures for dry powder inhalers, Int. J. Pharm. 541 (2018) 143–156.

[5] S.N. Bhattachar, D.B. Hedden, A.M. Olsofsky, X. Qu, W.-Y. Hsieh, K.G. Canter, Evaluation of the vibratory feeder method for assessment of powder flow properties, Int. J. Pharm. 269 (2004) 385–392.

[6] I.M. Zainuddin, M. Yasuda, T. Horio, S. Matsusaka, Experimental study on powder flowability using vibration shear tube method, Part. Part. Syst. Charact. 29 (2012) 8–15.

[7] T. Horio, M. Yasuda, S. Matsusaka, Measurement of flowability of lubricated powders by the vibrating tube method, Drug Dev. Ind. Pharm. 39 (2013) 1063–1069.

[8] T. Horio, M. Yasuda, S. Matsusaka, Effect of particle shape on powder flowability of microcrystalline cellulose as determined using the vibration shear tube method, Int. J. Pharm. 473 (2014) 572–578.

[9] M. Shoyama, T. Kawata, M. Yasuda, S. Matsusaka, Particle electrification and levitation in a continuous particle feed and dispersion system with vibration and external electric fields, Adv. Powder Technol. 29 (2018) 1960–1967.

[10] D. Macrì, D. Barletta, P. Lettieri, M. Poletto, Experimental and theoretical analysis of TiO$_2$ powders flow properties at ambient and high temperatures, Chem. Eng. Sci. 167 (2017) 172–190.

[11] Y. Liu, H. Lu, D. Barletta, M. Poletto, X. Guo, X. Gong, Y. Jin, Bulk flow properties of fly ashes at ambient and high temperature, Particuology 38 (2018) 113–125.

[12] V. Karde, D. Dixit, C. Ghoroi, Adhesion force approximation at varying consolidation stresses for fine powder under humid conditions, Adv. Powder Technol. 28 (2017) 346–355.

[13] S. Kamath, V.M. Puri, H.B. Manbeck, Flow property measurement using the Jenike cell for wheat flour at various moisture contents and consolidation times, Powder Technol. 81 (1994) 293–297.

[14] H. Lu, X. Guo, Y. Jin, X. Gong, Effect of moisture on flowability of pulverized coal, Chem. Eng. Res. Des. 133 (2018) 326–334.

[15] Y. Jin, H. Lu, X. Guo, X. Gong, Effect of water addition on flow properties of lignite particles, Chem. Eng. Res. Des. 132 (2018) 1020–1029.

[16] K. Takenaka, K. Iimura, M. Suzuki, M. Hirota, Shape effects of the yield locus on the Rankine coefficient, Adv. Powder Technol. 19 (2008) 25–37.

[17] W. Yu, K. Muteki, L. Zhang, G. Kim, Prediction of bulk powder flow performance using comprehensive particle size and particle shape distributions, J. Pharm. Sci. 100 (2011) 284–293.

[18] J. Mellmann, T. Hoffmann, C. Fürll, Flow properties of crushed grains as a function of the particle shape, Powder Technol. 249 (2013) 269–273.

[19] R.L. Carr, Evaluating flow properties of solids, Chem. Eng. January 18 (1965) 163–168.

[20] F. Lavoie, L. Cartilier, R. Thibert, New methods characterizing avalanche behavior to determine powder flow, Pharm. Res. 19 (2002) 887–893.

[21] A.W. Jenike, Gravity flow of bulk solids, Bull. Utah Eng. Exp. Stn. 52 (1961) 108.

[22] A.W. Jenike, Quantitative design of mass-flow bins, Powder Technol. 1 (1967) 237–244.

[23] M. Hirota, T. Kobayashi, T. Oshima, Proper test conditions for measurement by a direct shear tester with parallel plates, J. Soc. Powder Technol., Japan 20 (1983) 493–498.

[24] M. Hirota, T. Kobayashi, O. Sano, T. Oshima, Expansion and contraction behavior of a powder bed in a shear process, J. Soc. Powder Technol., Japan 21 (1984) 137–142.

[25] J. Schwedes, D. Schulze, Measurement of flow properties of bulk solids, Powder Technol. 61 (1990) 59–68.

[26] J. Schwedes, Review on testers for measuring flow properties of bulk solid, Granular Matter 5 (2003) 1–43.

[27] R. Freeman, Measuring the flow properties of consolidated, conditioned and aerated powders—a comparative study using a powder rheometer and a rotational shear cell, Powder Technol. 174 (2007) 25–33.

[28] R.J. Berry, M.S.A. Bradley, Investigation of the effect of test procedure factors on the failure loci and derived failure functions obtained from annular shear cells, Powder Technol. 174 (2007) 60–63.

[29] H. Tsunakawa, R. Aoki, Measurements of the failure properties of granular materials and cohesive powders, Powder Technol. 33 (1982) 249–256.

[30] H. Tsunakawa, R. Aoki, A direct shear test for powders and granular materials, J. Soc. Powder Technol., Japan 11 (1974) 263–268.

[31] H. Tsunakawa, Influence of consolidation stress upon yield loci of cohesive powders, J. Soc. Powder Technol., Japan 17 (1980) 61–67.

[32] Y. Shimada, S. Hatano, S. Matsusaka, A new method for evaluating powder flowability using constant-volume shear tester, J. Soc. Powder Technol., Japan 54 (2017) 90–96. Translated in Adv. Powder Technol. 29 (2018) 3577–3583. https://doi.org/10.1016/j.apt.2018.08.028.

[33] Y. Shimada, T. Kawata, S. Matsusaka, Analysis of constant-volume shear tests based on precise measurement of stresses in powder beds, Adv. Powder Technol. 29 (2018) 1372–1378.

[34] ASTM D6128, Standard test method for shear testing of bulk solids using the Jenike shear tester.

[35] ASTM D6773, Standard test method for bulk solids using Schulze ring shear tester.

[36] JIS Z 8835, Direct shear testing method for critical state line (CSL) and wall yield locus (WYL) of powder bed.

[37] J.W. Carson, H. Wilms, Development of an international standard for shear testing, Powder Technol. 167 (2006) 1–9.

[38] S. Koynov, B. Glasser, F. Muzzio, Comparison of three rotational shear cell testers: powder flowability and bulk density, Powder Technol. 283 (2015) 103–112.

[39] H. Salehi, D. Barletta, M. Poletto, A comparison between powder flow property testers, Particuology 32 (2017) 10–20.

[40] Y. Wang, S. Koynov, B.J. Glasser, F.J. Muzzio, A method to analyze shear cell data of powders measured under different initial consolidation stresses, Powder Technol. 294 (2016) 105–112.

[41] A. Vasilenko, B.J. Glasser, F.J. Muzzio, Shear and flow behavior of pharmaceutical blends—method comparison study, Powder Technol. 208 (2011) 628–636.

[42] Y. Wang, R.D. Snee, W. Meng, F.J. Muzzio, Predicting flow behavior of pharmaceutical blends using shear cell methodology: a quality by design approach, Powder Technol. 294 (2016) 22–29.

[43] S. Nakamura, N. Otsuka, Y. Yoshino, T. Sakamoto, H. Yuasa, Predicting the occurrence of sticking during tablet production by shear testing of a pharmaceutical powder, Chem. Pharm. Bull. 64 (2016) 512–516.

[44] E. Xanthakis, J.R. van Ommen, L. Ahrné, Flowability characterization of nanopowders, Powder Technol. 286 (2015) 156–163.